Breaking space-inversion symmetry in the dynamics of the doubly excited $Q_2\ ^1\Pi_u(1)$ state of HD

Kouichi Hosaka,[1,*] Yutaro Torizuka,[1] Philipp Schmidt,[2] Andre Knie,[2] Arno Ehresmann,[2] Takeshi Odagiri,[3] Masashi Kitajima,[1] and Noriyuki Kouchi[1]

[1]*Department of Chemistry, Tokyo Institute of Technology, Meguro-ku, Tokyo 152-8551, Japan*

[2]*Institute of Physics and Center for Interdisciplinary Nanostructure Science and Technology (CINSaT), University of Kassel, Heinrich-Plett-Straße 40, D-34132 Kassel, Germany*

[3]*Department of Materials and Life Sciences, Sophia University, Chiyoda-ku, Tokyo 102-8554, Japan*

(Received 19 November 2018; revised manuscript received 8 February 2019; published 28 March 2019)

A set of cross sections for the formation of a pair of $2p$ atoms on an absolute scale is determined against the incident photon energy in the double photoexcitation of the isotopomers H_2, HD, and D_2, incorporating the same cross sections of H_2 and D_2 obtained in our recent experiments [K. Hosaka *et al.*, Phys. Rev. A **93**, 063423 (2016)], and the oscillator strengths for the formation of a pair of $2p$ atoms from the precursor $Q_2\ ^1\Pi_u(1)$ state, $f_{2p2p}^{H_2/HD/D_2}(Q_2\ ^1\Pi_u(1))$, are determined from the cross sections. The oscillator strength of HD, $f_{2p2p}^{HD}(Q_2\ ^1\Pi_u(1))$, is found to be larger than the value expected from $f_{2p2p}^{H_2/D_2}(Q_2\ ^1\Pi_u(1))$, considering the same decay mechanism for H_2, HD, and D_2 molecules photoexcited to the $Q_2\ ^1\Pi_u(1)$ state, a mechanism which was revealed in our recent experiments for H_2 and D_2 mentioned above. The origin of the enhancement in the oscillator strength for HD is discussed and we show that the enhancement is attributed to nonadiabatic transitions between a gerade electronic state and an ungerade one through a term neglected in the Born-Oppenheimer approximation that vanishes in the homonuclear isotopomers (H_2 and D_2) but does not vanish in the heteronuclear isotopomer (HD). It turns out that approximately 10–20 % of $f_{2p2p}^{HD}(Q_2\ ^1\Pi_u(1))$ originates from such nonadiabatic transitions due to the breaking of the space-inversion symmetry for electrons.

DOI: 10.1103/PhysRevA.99.033423

I. INTRODUCTION

Doubly excited states of atoms and molecules are embedded in ionization continua and superposed with the continuous electronic states with nearly the same energy [1], in contrast to excited electronic states below the ionization energy. The superposition of a discrete electronic state and nearby continuous electronic states results in the autoionization of atoms and molecules. As for molecular doubly excited states, another point should be noted: They are not separated into electronic and nuclear parts due to this superposition, i.e., they are not described with the Born-Oppenheimer products [2,3]. The dynamics of doubly excited molecules have thus been an attractive subject for research for these aspects, in particular, for hydrogen molecules [4–20], which have the advantage that the repulsive potential energy curves and resonance widths of doubly excited states, fundamental quantities in the investigation of their dynamics, have been intensively calculated, in contrast to other molecules [21–28]. The dynamics of doubly excited hydrogen molecules, however, have not been fully understood. The dynamics of the forbidden doubly excited states have been less studied than the allowed ones, e.g., the origin of a forbidden peak found in the electron energy loss spectra of H_2 [29] and D_2 [30] tagged with $2p$ atom formation remains unidentified [12]. Another issue is related to the breaking of the space-inversion symmetry, which is an interesting and important phenomenon in atomic and molecular physics [31]. Although the breaking of the space-inversion symmetry is expected to be observed in the dynamics of the doubly excited HD molecules, as discussed in the following, the breaking has not been substantiated.

In H_2 and D_2 as well as HD molecules, the nuclear charges are the same and the electronic states are hence labeled gerade or ungerade according to the eigenvalues of the space-inversion operator for electrons within the Born-Oppenheimer approximation. The interaction between a gerade state and an ungerade state of diatomic molecules, abbreviated as the *g-u* interaction, is forbidden (see, e.g., Table 3.2 on p. 97 in Ref. [32]) within the Born-Oppenheimer approximation, but in fact the weak *g-u* interaction occurs because, as discussed in Sec. III C, a term that does not commute with the space-inversion operator for electrons is added to the total Hamiltonian of a diatomic molecule of interest to the higher-order approximation, a term which does not vanish for HD but vanishes for H_2 and D_2. The *g-u* interaction, a result of the breaking of the space-inversion symmetry, is hence characteristic of the heteronuclear isotopomer HD and is forbidden in the homonuclear isotopomers H_2 and D_2. Based on the discussion above, it becomes a significant subject to experimentally separate one doubly excited state from among various doubly excited states of these isotopomers and determine the role of the breaking of the space-inversion symmetry in the dynamics of the doubly excited state through a comparison among H_2, HD, and D_2 based on the fact that the breaking of the space-inversion symmetry occurs for HD but does not occur for H_2 and D_2.

From the experimental side, the key to observing the doubly excited states is extracting the discrete electronic states

*hosakak@chem.titech.ac.jp

from the superposition with continuous electronic states [33]. We have hence determined cross sections for the emission of fluorescence from neutral fragments as functions of excitation energy [5,6,12,20] since the detection of such fluorescence photons, in contrast to the detection of charged species, excludes the contribution of the continuous electronic states and the contribution of the discrete electronic state is naturally extracted as a result. Following this line, we investigated the dynamics of the doubly excited $Q_2\ ^1\Pi_u(1)$ state by determining the cross sections for the formation of a pair of $2p$ atoms against the incident photon energy in the range 30–40 eV in the photoexcitation of H_2 and D_2 [5,20]; this formation is abbreviated to $2p+2p$ pair formation in the present paper. Only the $Q_2\ ^1\Pi_u(1)$ state was observed in the cross-section curve, taking advantage of the coincidence detection of two Lyman-α photons, in contrast to the detection of a single Lyman-α photon [7,13], and the decay mechanism of the state was identified (see the blue arrows in Fig. 3). A clear isotope effect was seen, i.e., the oscillator strength for $2p+2p$ pair formation in D_2 is 0.69 times that in H_2, which was explained by the competition around the Franck-Condon region between the mass-independent autoionization rate and mass-dependent neutral-dissociation rate for hydrogen molecules dissociating down the repulsive potential energy curve of the $Q_2\ ^1\Pi_u(1)$ state [20].

In the present experiment we determine the cross sections for $2p+2p$ pair formation against the incident photon energy in the photoexcitation of HD and compare the cross sections with those in the photoexcitation of H_2 and D_2 [20] to study the role of nonadiabatic transitions between gerade and ungerade electronic states in the oscillator strength for $2p+2p$ pair formation from the photoexcited $Q_2\ ^1\Pi_u(1)$ state of HD. Those transitions are brought about by the breaking of the space-inversion symmetry and are abbreviated as *g-u* nonadiabatic transitions.

The *g-u* interaction was extensively studied in rovibrational levels of singly excited states of HD by means of high-resolution spectroscopy as reviewed in [31]. The interaction was also found in the study of predissociation rates in $^7Li^7Li$, $^6Li^6Li$, and $^6Li^7Li$ dimers [34,35] and the study of the intensities in the high-resolution inner-shell photoelectron spectra of $^{14}N^{14}N$, $^{15}N^{15}N$, and $^{14}N^{15}N$ molecules [36]. Here we study the dynamical effect of the breaking of the space-inversion symmetry due to the isotope substitution for the doubly excited states.

II. EXPERIMENT

Cross sections for $2p+2p$ pair formation in the photoexcitation of HD have been measured at the bending beamline BL-20A of the Photon Factory, KEK, equipped with a 3-m normal-incidence monochromator [37]. The experimental apparatus is the same as that used to measure the same cross sections for H_2 and D_2 in our recent experiments [20] and is hence discussed briefly below.

A. Outline of the apparatus

Linearly polarized light was introduced into a gas cell filled with the sample gas. The HD gas was purchased from Cambridge Isotope Laboratories, Inc. and its chemical and isotope purities were 98% and 97%, respectively. A pair of Lyman-α photons was detected in coincidence by two detectors, which were fitted to the gas cell and placed on the plane perpendicular to the incident light beam. The detectors on the plane were positioned to face in opposite directions and aligned on the line perpendicular to the unit polarization vector of the linearly polarized incident light. The coincidence measurement was carried out at a given energy (ranging from 30 to 40 eV) of the incident photon with the coincidence system shown in Ref. [20]. The bandpass of the wavelength of the incident light was 0.14 nm (an energy width of 140 meV at an incident photon energy of 35 eV). The flux of the incident photons was measured at the exit of the gas cell by measuring the photocurrent of an Au plate. The sensitivity of the Au plate was obtained against the incident photon energy with successive measurements of photocurrents of the Au plate and silicon photodiode (model AXUV-100G, IRD Inc.). The sensitivity of the latter was provided by NIST.

B. Photon detectors

Each photon detector for the vacuum ultraviolet radiation is comprised of a 1-mm-thick MgF_2 window and microchannel plate (F4655-10, Hamamatsu photonics) coated with CsI, which provides a filter range of approximately 115–200 nm in wavelength. Only the Lyman-α fluorescence, with a 121.6-nm wavelength for H atoms, is detected in the present range of incident photon energy, 30–40 eV, for the following reason: Since doubly excited hydrogen molecules produced with photoexcitation decay through autoionization and neutral dissociation and excited H_2^+ (HD^+ and D_2^+) ions decay through dissociation with the contribution of the fluorescent process from both species being negligible, fluorescence is emitted by excited hydrogen atoms alone. The Lyman-α fluorescence penetrates the 1-mm-thick MgF_2 window while the Lyman-β fluorescence, with a 102.6-nm wavelength for H atoms, does not penetrate as well as other Lyman fluorescences. Other fluorescence of atomic hydrogen besides the Lyman series does not lie in the vacuum ultraviolet range.

C. Determination of the cross sections for $2p+2p$ pair formation

The procedure for determining the absolute values of the cross sections for $2p+2p$ pair formation in the photoexcitation of HD is the same as that in the photoexcitation of H_2 and D_2 discussed in detail in Ref. [20] and only the outline is given here. A two-photon coincidence time spectrum was recorded at a given energy of the incident photon E with the coincidence system shown in Ref. [20], from which spectrum a two-photon coincidence count rate $\dot{N}_{cd}(E,\Theta_c,\Theta_d)$ was obtained following the manner given in Ref. [20]. The angles Θ_c and Θ_d express the directions of the photon detectors c and d, respectively, with respect to the unit polarization vector of the incident light. It was found in our recent experiments [20] that the two-photon coincidence rate is proportional to the D_2 gas pressure in the gas cell up to 2.0 Pa. The HD gas pressure is thus kept lower than approximately 1 Pa in the present experiments. The two-photon

coincidence count rate $\dot{N}_{cd}(E, \Theta_c, \Theta_d)$ in the photoexcitation of hydrogen molecules in such a pressure range where the proportional relation with the target gas pressure is seen is related to the angle-differential cross section for the emission of a pair of the Lyman-α photons averaged with the angular resolution $\langle q\rangle(E, \Theta_c, \Theta_d)$ [20],

$$\dot{N}_{cd}(E, \Theta_c, \Theta_d) = 2n\left(\frac{I'(E)G_{cd}(\Theta_c, \Theta_d)}{A}\right)\eta_{cd}\langle q\rangle(E, \Theta_c, \Theta_d), \tag{1}$$

where n is the number density of target molecules, $I'(E)$ the flux of the incident photons, A the cross-section area of the incident photon beam, $G_{cd}(\Theta_c, \Theta_d)$ the geometric factor, and η_{cd} the coincidence detection efficiency of the photon detectors for the Lyman-α photons. The geometric factor $G_{cd}(\Theta_c, \Theta_d)$ is in fact independent of (Θ_c, Θ_d), as discussed in Ref. [17]. It is also independent of the incident photon energy E since the position and shape of the incident light beam do not change quite as much in the present range of incident photon energy. For the same reason, A is independent of E. The flux of the incident photons $I'(E)$ is related to the photocurrent of the Au plate $i_{\rm Au}(E)$ as

$$I'(E) = CK(E)i_{\rm Au}(E), \tag{2}$$

where C is a constant independent of E. The function $K(E)$, which is related to the sensitivity of the Au plate as a function of incident photon energy, was obtained with the successive measurements of photocurrents of the Au plate and silicon photodiode as discussed in Sec. II A.

According to Eqs. (1) and (2), the coincidence count rate $\dot{N}_{cd}(E, \Theta_c, \Theta_d)$ is normalized for the target gas pressure and flux of incident photons and the normalized rate is denoted by $S_{cd}(E, \Theta_c, \Theta_d)$,

$$S_{cd}(E, \Theta_c, \Theta_d) = \frac{\dot{N}_{cd}(E, \Theta_c, \Theta_d)}{P[K(E)i_{Au}(E)]}, \tag{3}$$

where P is the pressure of target molecules in the gas cell. The normalized count rate S_{cd} defined in Eq. (3) is related to the angle-differential cross sections $\langle q\rangle$ by

$$S_{cd}(E, \Theta_c, \Theta_d) = \frac{2}{k_BT}\frac{CG_{cd}(\Theta_c, \Theta_d)}{A}\eta_{cd}\langle q\rangle(E, \Theta_c, \Theta_d), \tag{4}$$

where T is the temperature of the target gas, the room temperature in this experiment, and k_B is the Boltzmann constant. The plot of the values of $S_{cd}(E, \Theta_c, \Theta_d)$ against the incident photon energy E with the angle Θ_c and Θ_d held fixed hence shows the plot of the cross section $\langle q\rangle(E, \Theta_c, \Theta_d)$ against E on a relative scale of the vertical axis.

In fact, however, we carry out the reference measurements at a constant energy of the incident photon $E^{\rm ref}$ to compensate for a possible but small and slow change of the geometric factor $G_{cd}(\Theta_c, \Theta_d)$, the sensitivity of the detectors η_{cd}, the cross-section area A, and the factor C in Eq. (4) during the measurement of $\langle q\rangle$ against E. Reference measurements are carried out before and after the measurement of $\dot{N}_{cd}(E, \Theta_c, \Theta_d)$ so that $\dot{N}^b_{cd}(E^{\rm ref}, \Theta_c, \Theta_d)$ and $\dot{N}^a_{cd}(E^{\rm ref}, \Theta_c, \Theta_d)$, respectively, are obtained, and the following relation is derived:

$$\frac{S_{cd}(E, \Theta_c, \Theta_d)}{\frac{1}{2}\left[S^b_{cd}(E^{\rm ref}, \Theta_c, \Theta_d) + S^a_{cd}(E^{\rm ref}, \Theta_c, \Theta_d)\right]} = \frac{\langle q\rangle(E, \Theta_c, \Theta_d)}{\langle q\rangle(E^{\rm ref}, \Theta_c, \Theta_d)}. \tag{5}$$

In deriving Eq. (5) the factor $\frac{CG_{cd}(\Theta_c,\Theta_d)\eta_{cd}}{A}$ in Eq. (4) is considered unchanged during the measurements of $\dot{N}^b_{cd}$, $\dot{N}_{cd}$, and $\dot{N}^a_{cd}$. We eventually plot the values on the left-hand side of Eq. (5) against the incident photon energy E with the angle Θ_c and Θ_d held fixed at $-90°$ and $90°$, respectively, as mentioned in Sec. II A, so that the relative values of $\langle q\rangle(E, -90°, 90°)$ are shown against E. The value of $E^{\rm ref}$ was chosen to be 33.66 eV, as in our recent experiments [20].

The coincidence count rates for H_2 and HD at $E^{\rm ref}$, i.e., $\dot{N}^{H_2}_{cd}(E^{\rm ref}, -90°, 90°)$ and $\dot{N}^{\rm HD}_{cd}(E^{\rm ref}, -90°, 90°)$, respectively, have been sequentially measured so that the ratio of $\langle q^{H_2}\rangle(E^{\rm ref}, -90°, 90°)$ and $\langle q^{\rm HD}\rangle(E^{\rm ref}, -90°, 90°)$ has been obtained with the factor $\frac{CG_{cd}(\Theta_c,\Theta_d)\eta_{cd}}{A}$ in Eq. (4) again considered unchanged during the measurement. We multiply the cross-section ratio $\langle q^{\rm HD}\rangle(E, -90°, 90°)/\langle q^{\rm HD}\rangle(E^{\rm ref}, -90°, 90°)$, obtained according to Eq. (5), by the ratio $\langle q^{\rm HD}\rangle(E^{\rm ref}, -90°, 90°)/\langle q^{\rm H_2}\rangle(E^{\rm ref}, -90°, 90°)$ to obtain the values of $\langle q^{\rm HD}\rangle(E, -90°, 90°)/\langle q^{\rm H_2}\rangle(E^{\rm ref}, -90°, 90°)$ against the incident photon energy E. In our recent experiments for H_2 and D_2 [20], the values of $\langle q^{\rm H_2/D_2}\rangle(E, -90°, 90°)/\langle q^{\rm H_2}\rangle(E^{\rm ref}, -90°, 90°)$ were obtained against E. As seen above, the denominator $\langle q^{H_2}\rangle(E^{\rm ref}, -90°, 90°)$ is common throughout the H_2, HD, and D_2 experiments.

The values of $\langle q^M\rangle(E, -90°, 90°)/\langle q^{H_2}\rangle(E^{\rm ref}, -90°, 90°)$ ($M = H_2$, HD, and D_2) are almost equal to those of

$$\sigma^M_{2p2p}(E)/\sigma^{H_2}_{2p2p}(E^{\rm ref})$$

where $\sigma^M_{2p2p}(E)$ are the cross sections for $2p + 2p$ pair formation to be determined in the photoexcitation of M (=H_2, HD, and D_2), because of the following reason. Angular correlation functions of a pair of Lyman-α photons were measured at 33.66-eV incident photon energy for H_2 [17], HD [38], and D_2 [38] and it was found that the isotope effect on the angular correlation function is negligible and the angular correlation is not so strong for each molecule. The angular correlation function in the photoexcitation of H_2 and D_2 is likely to be independent of the incident photon energy in the range 30–40 eV since only the $Q_2\ ^1\Pi_u(1)$ state is involved in $2p + 2p$ pair formation [20]. The energy-independent angular correlation also seems to be the case for HD because of the dominant contribution of the $Q_2\ ^1\Pi_u(1)$ state in HD, which is discussed in Sec. III. It hence follows that the values of $\langle q^M\rangle(E, -90°, 90°)/\langle q^{H_2}\rangle(E^{\rm ref}, -90°, 90°)$ are almost equal to those of $\sigma^M_{2p2p}(E)/\sigma^{H_2}_{2p2p}(E^{\rm ref})$. By simply obtaining the absolute value of $\sigma^{H_2}_{2p2p}(E^{\rm ref})$, we are hence able to determine the absolute values of $\sigma^M_{2p2p}(E)$ for M (=H_2, HD, and D_2). The method for obtaining the absolute value of $\sigma^{H_2}_{2p2p}(E^{\rm ref})$ was described in detail in Ref. [20] and is based on the quantum yields of $H(2s)$ formation and $H(2p)$ formation from the $Q_2\ ^1\Pi_u(1)$ state of H_2 [7] and the oscillator strength for $H(2s)$ formation from the $Q_2\ ^1\Pi_u(1)$ state of H_2 [14]. The absolute values of $\sigma^{\rm HD}_{2p2p}(E)$ are thereby determined against the incident

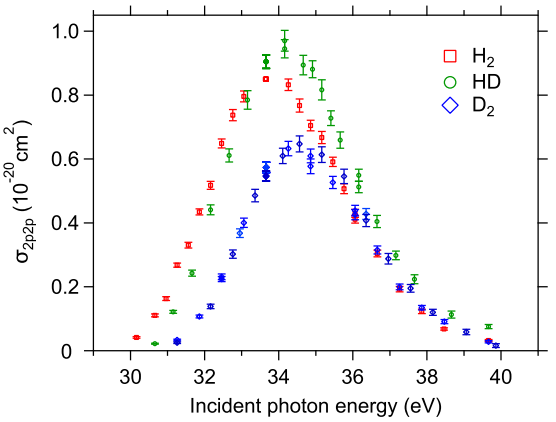

FIG. 1. Plot of cross sections for $2p+2p$ pair formation in the photoexcitation of H_2 (□), HD (○), and D_2 (◇) against the incident photon energy.

photon energy in this experiment. The values of $\sigma^{H_2}_{2p2p}(E)$ and $\sigma^{D_2}_{2p2p}(E)$ have also been determined at many energies of the incident photon in addition to those energies where the cross sections were determined in our recent experiments [20] because more data points enable us to obtain a more accurate value of the oscillator strength for $2p+2p$ pair formation. We note that the validity of the present procedure for obtaining the absolute values of $\sigma_{2p2p}(E)$ was substantiated through comparing the experimental $S(E^{\rm ref}, -90°, 90°)$ for D_2 in Eq. (3) and that calculated following Eq. (4) from the simulated value of G_{cd}/A, expected values of η_{cd} and C, and the value of $\sigma^{D_2}_{2p2p}(E^{\rm ref})$ determined in the present way [the approximate relation $\sigma^{D_2}_{2p2p}(E^{\rm ref})/(4\pi)^2 = \langle q^{D_2}\rangle(E^{\rm ref}, -90°, 90°)$ was used because of the weak angular anisotropy in the emission of Lyman-α photon pairs [38] mentioned before] [20].

III. RESULTS AND DISCUSSION

In Fig. 1 the absolute values of the cross sections for $2p+2p$ pair formation in the photoexcitation of HD, $\sigma^{HD}_{2p2p}(E)$, are plotted against the incident photon energy E. Those in H_2, $\sigma^{H_2}_{2p2p}(E)$, and D_2, $\sigma^{D_2}_{2p2p}(E)$, are also plotted (many points for H_2 and D_2 have been added to those obtained in our recent experiments [20]). The error bar is attributed to the statistical uncertainty of the two-photon coincidence count rates involved in the procedure discussed in Sec. II C.

As mentioned in Ref. [20], the precursor doubly excited state of the $2p+2p$ pair is the $Q_2\,{}^1\Pi_u(1)$ state for H_2 and D_2, and the decay mechanism of H_2 and D_2 molecules photoexcited to the $Q_2\,{}^1\Pi_u(1)$ state has been identified as shown with the blue arrows in Fig. 3: (i) H_2 (D_2) molecules photoexcited to the $Q_2\,{}^1\Pi_u(1)$ state in the Franck-Condon region dissociate down its repulsive potential curve (the blue horizontal solid arrow) and (ii) a proportion of the molecules transfer to the $Q_2\,{}^1\Pi_u(2)$ state around the internuclear distance of $5.6a_0$ through the nonadiabatic radial coupling (the blue vertical arrow) and then dissociate down the repulsive potential curve of the $Q_2\,{}^1\Pi_u(2)$ state into the $2s+2p$ pairs (the blue horizontal dashed arrow) while the rest of the molecules remain dissociating down the repulsive potential curve of the $Q_2\,{}^1\Pi_u(1)$ state into the $2p+2p$ pairs (the blue horizontal solid arrow again). The shape of the cross-section curve for HD is similar to those of H_2 and D_2, hence we conclude that the cross-section curve for HD is again attributed to the doubly excited $Q_2\,{}^1\Pi_u(1)$ state. The peak energy for HD is higher than that for H_2 by 350 meV and the peak energy for D_2 is higher than that for HD by 450 meV. The ascending order of the peak energies is in reasonable accord with the descending order of the zero-point energies in the ground electronic state of hydrogen molecules, but the magnitude of the difference in the peak energies is not accounted for by the difference in the zero-point energies alone: The zero-point energy in HD is lower than that in H_2 by 36 meV and the zero-point energy in D_2 is lower than that in HD by 43 meV [39].

TABLE I. Experimental oscillator strengths of $2p+2p$ pair formation from the $Q_2\,{}^1\Pi_u(1)$ state, $f_{2p2p}(Q_2\,{}^1\Pi_u(1))$, in the photoexcitation of H_2, HD, and D_2. They have been obtained through integrating the cross-section curves in Fig. 1 over the incident photon energy [20]. The ratio of the relative velocities of the two nuclei is shown for the discussion in Sec. III A.

Isotopomer	$f_{2p2p}(Q_2\,{}^1\Pi_u(1))$	Ratio of nuclear relative velocities
H_2	$(3.5\pm0.1)\times10^{-4}$	1
HD	$(3.8\pm0.1)\times10^{-4}$	0.87
D_2	$(2.5\pm0.1)\times10^{-4}$	0.71

A. General discussion about the isotope effect on the oscillator strengths for $2p+2p$ pair formation

The oscillator strengths of $2p+2p$ pair formation from the $Q_2\,{}^1\Pi_u(1)$ state, $f_{2p2p}(Q_2\,{}^1\Pi_u(1))$, have been obtained through integrating the cross-section curves in Fig. 1 over the incident photon energy E (see Ref. [20] for details) and are summarized in Table I. The clear isotope effect between H_2 and D_2 in Table I is explained as a consequence of the competition between the electronic autoionization and neutral dissociation from the $Q_2\,{}^1\Pi_u(1)$ state as discussed below [20]. The potential energy curve and resonance width of a doubly excited state have no isotope effects and the latter gives the rate of electronic autoionization. On the other hand, the relative velocity of two nuclei separating down the potential energy curve in D_2 is $1/\sqrt{2}$ (=0.71) times that in H_2 (see Table I) and D_2 thus needs more time to reach the region of the internuclear distance of zero or a small resonance width than H_2. As a result, D_2 has a lower probability of escaping from the autoionization than H_2. The oscillator strength of an electronic excitation has just a small isotope effect since the sum of the Franck-Condon factors of the electronic excitation is equal to unity, as discussed in Ref. [20]. In general, the heavier isotope substitution thus makes the state-resolved oscillator strength of neutral dissociation smaller and makes the state-resolved oscillator strength of autoionization larger. The isotope effect between H_2 and D_2 in Table I is qualitatively explained in this way. Based on this discussion and the fact that the relative velocity of the two nuclei in HD is $\sqrt{3}/2 = 0.87$ times that in H_2 (see Table I), the oscillator strength for

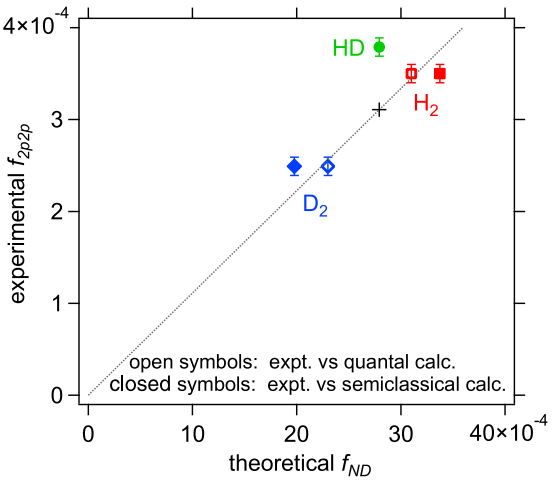

FIG. 2. Correlation between the experimental oscillator strengths of $2p+2p$ pair formation from the $Q_2\ ^1\Pi_u(1)$ state, $f_{2p2p}(Q_2\ ^1\Pi_u(1))$, and those of neutral dissociation from the $Q_2\ ^1\Pi_u(1)$ state, $f_{\rm ND}(Q_2\ ^1\Pi_u(1))$, calculated in the quantal manner [40–42] (open symbols) and the semiclassical manner in this study (closed symbols). The dotted line is the best result of fitting the proportional relation to the two open symbols. Red squares are for H_2, green circles for HD, and blue diamonds for D_2 (the symbols are the same as in Fig. 1). The plus shows the value of $f_{2p2p}(Q_2\ ^1\Pi_u(1))$ for HD expected from those for H_2 and D_2 based on the assumption that the decay mechanisms of hydrogen molecules photoexcited to the $Q_2\ ^1\Pi_u(1)$ state are the same for H_2, HD, and D_2.

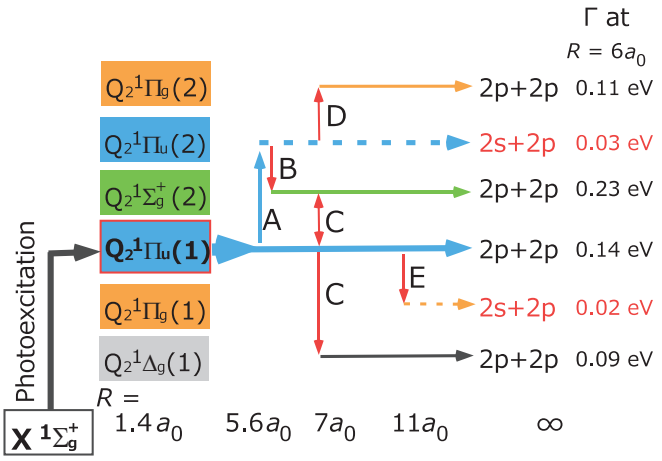

FIG. 3. Schematic diagram showing the possible doubly excited states and nonadiabatic transitions that may influence the values of $f_{2p2p}(Q_2\ ^1\Pi_u(1))$ in the photoexcitation of H_2, HD, and D_2 to the $Q_2\ ^1\Pi_u(1)$ state. The potential energy curves of the doubly excited states are repulsive and the horizontal arrows denote the adiabatic dissociation channels [26], while the vertical arrows denote the nonadiabatic transitions at the indicated internuclear distances R. The red vertical arrows show the g-u nonadiabatic transitions due to the $\hat{H}_{g\text{-}u}$ term and the blue vertical arrows the nonadiabatic transitions due to the radial coupling. The blue channels starting from the $Q_2\ ^1\Pi_u(1)$ state, shown by the blue horizontal and blue vertical arrows, have been substantiated for H_2 and D_2 [20]. The resonance width Γ at the internuclear distance of $6a_0$ is shown for each doubly excited state [23].

HD seems larger than the value expected from H_2 and D_2, which is substantiated in the following section.

B. Enhanced oscillator strength for $2p+2p$ pair formation in HD

Figure 2 shows a correlation between the experimental values of $f_{2p2p}(Q_2\ ^1\Pi_u(1))$ and the theoretical oscillator strengths of the neutral dissociation from the $Q_2\ ^1\Pi_u(1)$ state, $f_{\rm ND}(Q_2\ ^1\Pi_u(1))$. The neutral dissociation means escaping from the autoionization in the $Q_2\ ^1\Pi_u(1)$ state and the theoretical $f_{\rm ND}(Q_2\ ^1\Pi_u(1))$ hence reflects the competition between the mass-independent autoionization rate and the mass-dependent neutral dissociation rate, which is the origin of the isotope effect as discussed in Sec. III A. The values of $f_{\rm ND}(Q_2\ ^1\Pi_u(1))$ were calculated by solving the time-dependent Schrödinger equation of H_2 and D_2 under a photon field [40–42], with nonadiabatic transitions not being taken into account. The correlation between the experimental $f_{2p2p}(Q_2\ ^1\Pi_u(1))$ and the theoretical $f_{\rm ND}(Q_2\ ^1\Pi_u(1))$ [40–42] is shown for H_2 and D_2 in Fig. 2 (open symbols), where both open symbols align well on a line passing through the origin (dotted line). A good correlation has been found for H_2 and D_2, which is likely to be attributed to the fact that the decay mechanisms of hydrogen molecules photoexcited to the $Q_2\ ^1\Pi_u(1)$ state are the same for H_2 and D_2, as shown with the blue arrows in Fig. 3 [20]; the autoionization rates of the $Q_2\ ^1\Pi_u(1)$ state are also the same, but the relative velocities of two nuclei down the repulsive potential curve of the $Q_2\ ^1\Pi_u(1)$ state are different because of the difference in the nuclear masses in H_2 and D_2 (see Table I). The slope of the dotted line is much less than unity, which is consistent with our result that the oscillator strengths for $2s+2p$ pair formation from the $Q_2\ ^1\Pi_u(1)$ state of H_2 and D_2 are about 6 times those for $2p+2p$ pair formation from the same state of H_2 and D_2, respectively [20].

Unfortunately, $f_{\rm ND}(Q_2\ ^1\Pi_u(1))$ has not been calculated for HD with the method like the quantal one described in Refs. [40–42]. We hence use a semiclassical manner for calculating the values of $f_{\rm ND}(Q_2\ ^1\Pi_u(1))$ for H_2, HD, and D_2, as discussed below. The probability that hydrogen molecules in the $Q_2\ ^1\Pi_u(1)$ state escape from the autoionization during the classical motion of the separating nuclei from the equilibrium internuclear distance $1.4a_0$ to the internuclear distance of $5.6a_0$ [20] has been calculated for H_2, HD, and D_2 in the present study following the way given in Refs. [30,43,44]; these probabilities are referred to as the survival probabilities and are denoted by $s(Q_2\ ^1\Pi_u(1))$,

$$s(Q_2\ ^1\Pi_u(1)) = \exp\left(-\int_{R=1.4a_0}^{R=5.6a_0} \frac{\Gamma(R)}{\hbar v'(R)} dR\right), \quad (6)$$

$$v'(R) = \left(\frac{1}{2}\left\{[v(R)]^2 + \left[[v(R)]^4 + \left(\frac{\Gamma(R)}{\mu}\right)^2\right]^{1/2}\right\}\right)^{1/2}, \quad (7)$$

where $\Gamma(R)$ is the resonance width of the $Q_2\ ^1\Pi_u(1)$ state against the internuclear distance R [23], $v(R)$ is the radial velocity of the relative motion of the two nuclei, and μ is the reduced mass of the two nuclei. The radial velocity $v(R)$ is

related to the potential energy curve $V(R)$ of the $Q_2\ ^1\Pi_u(1)$ state [23] as

$$v(R) = \left(\frac{2[V(1.4a_0) - V(R)]}{\mu}\right)^{1/2}. \tag{8}$$

As mentioned in Ref. [20], the ratio of the survival probabilities $s^{D_2}(Q_2\ ^1\Pi_u(1))/s^{H_2}(Q_2\ ^1\Pi_u(1))$ accounts for the isotope effect of the experimental oscillator strengths of $2p+2p$ pair formation in Table I, $f^{D_2}_{2p2p}(Q_2\ ^1\Pi_u(1))/f^{H_2}_{2p2p}(Q_2\ ^1\Pi_u(1))$. The photoabsorption cross section for the excitation to the $Q_2\ ^1\Pi_u(1)$ state of H_2 was calculated [45] and the oscillator strength for the excitation in H_2, $f_{ex}(Q_2\ ^1\Pi_u(1))$, has been easily obtained by integrating the photoabsorption cross section over the incident photon energy. As mentioned in Sec. III A, the excitation oscillator strength has just a small isotope effect. Eventually, the values of $f_{ex}(Q_2\ ^1\Pi_u(1))s^{H_2/HD/D_2}(Q_2\ ^1\Pi_u(1))$ are calculated, which give the theoretical $f_{ND}(Q_2\ ^1\Pi_u(1))$ for H_2, HD, and D_2, respectively.

It has been found that the values of $f_{ex}(Q_2\ ^1\Pi_u(1))s(Q_2\ ^1\Pi_u(1))$ for H_2 and D_2 calculated in this study in the semiclassical manner are not in agreement with those of $f_{ND}(Q_2\ ^1\Pi_u(1))$ for H_2 and D_2 calculated in the quantal manner [40–42], respectively; this disagreement is probably due to the semiclassical treatment of the decay of the $Q_2\ ^1\Pi_u(1)$ state in calculating the survival probabilities $s(Q_2\ ^1\Pi_u(1))$. The values of $f_{ex}(Q_2\ ^1\Pi_u(1))s(Q_2\ ^1\Pi_u(1))$ for H_2 and D_2 multiplied by a common factor 1.82, however, almost equal those of $f_{ND}(Q_2\ ^1\Pi_u(1))$ for H_2 and D_2 calculated in the quantal manner [40–42], respectively, and hence we conclude that $1.82 f_{ex}(Q_2\ ^1\Pi_u(1))s(Q_2\ ^1\Pi_u(1))$ calculated in this study for HD is a good approximation of the $f_{ND}(Q_2\ ^1\Pi_u(1))$ for HD, which have not been calculated in the same quantal manner as in Refs. [40–42].

The correlation between the experimental values of $f_{2p2p}(Q_2\ ^1\Pi_u(1))$ and $1.82 f_{ex}(Q_2\ ^1\Pi_u(1))s(Q_2\ ^1\Pi_u(1))$ calculated in this study is also shown in Fig. 2 for H_2, HD, and D_2 (closed symbols) in addition to the correlation between the experimental results and the theoretical $f_{ND}(Q_2\ ^1\Pi_u(1))$ for H_2 and D_2 calculated in the quantal manner [40–42] (open symbols). While the points for H_2 and D_2 (the closed red and closed blue symbols) almost align on the dotted line, the point for HD (the closed green circle) deviates much more from the dotted line along the vertical axis than the H_2 point (the closed red square) and the D_2 point (the closed blue diamond) do. As mentioned before, the good correlation for H_2 and D_2 (the red and blue symbols) is likely to be attributed to the fact that the decay mechanisms of hydrogen molecules photoexcited to the $Q_2\ ^1\Pi_u(1)$ state are the same for H_2 and D_2, as shown with the blue arrows in Fig. 3 [20]; the autoionization rates of the $Q_2\ ^1\Pi_u(1)$ state are also the same, but the relative velocities of two nuclei down the repulsive potential curve of the $Q_2\ ^1\Pi_u(1)$ state are different (see Table I). Assuming that the decay mechanism of HD molecules photoexcited to the $Q_2\ ^1\Pi_u(1)$ state is the same as that for H_2 and D_2 (the blue arrows in Fig. 3), the correlation that is the same as the good correlation for H_2 and D_2 is expected for H_2, HD, and D_2 as well, and the value of $f_{2p2p}(Q_2\ ^1\Pi_u(1))$ for HD is hence expected to be nearly 3.1×10^{-4}, as shown by the plus in Fig. 2. In fact, however, the experimental $f_{2p2p}(Q_2\ ^1\Pi_u(1))$ is clearly larger than that value, a result that is referred to as the enhancement in the oscillator strength, and it is reasonable that the enhancement in the oscillator strength for HD is attributed to the appearance of new dissociation channels other than the blue arrows in Fig. 3, channels which contribute to $2p+2p$ pair formation and can be accessed from the $Q_2\ ^1\Pi_u(1)$ state only for HD. As mentioned at the beginning of this section, the appearance of new precursor states other than the $Q_2\ ^1\Pi_u(1)$ state in the photoexcitation of HD has been ruled out. In the following section we identify the new dissociation channels, which occur in HD but do not occur in H_2 and D_2.

C. Origin of the enhancement in the oscillator strength for $2p+2p$ pair formation in HD

In the Born-Oppenheimer approximation the mass of electrons in a molecule is considered negligible in comparison with those of nuclei and we hence neglect the small deviation between the center of mass of the molecule composed of electrons and nuclei and that of the nuclei alone (see Ref. [32], p. 89, and Refs. [46,47]). In fact, this deviation gives the total Hamiltonian for molecules additional terms that are neglected in the Born-Oppenheimer approximation [46,47]. To see the additional terms in brief, we consider a diatomic molecule composed of nuclei a and b, of masses M_a and M_b, respectively, together with N electrons, labeled $1, 2, \ldots, N$. Following Refs. [46,47], the term $\hat{H}'$ to be added to the nonrelativistic total Hamiltonian under the Born-Oppenheimer approximation is expressed as

$$\hat{H}' = -\frac{\hbar^2}{2\mu_\alpha}\nabla_{\boldsymbol{R}} \cdot \sum_{i=1}^{N} \nabla_{\boldsymbol{r}_i} - \frac{\hbar^2}{8\mu} \sum_{i,j=1}^{N} \nabla_{\boldsymbol{r}_i} \cdot \nabla_{\boldsymbol{r}_j}, \tag{9}$$

$$\mu_\alpha = \frac{M_b M_a}{M_b - M_a}, \tag{10}$$

$$\mu = \frac{M_b M_a}{M_b + M_a}. \tag{11}$$

In Eq. (9), the origin is taken at the midpoint between the nuclei, $\boldsymbol{R}$ denotes the relative position vector of the nuclei, and $\boldsymbol{r}_i$ denotes the position vector of the ith electron. The nonrelativistic total Hamiltonian H is thus written as

$$\hat{H} = -\frac{\hbar^2}{2m_e}\sum_{i=1}^{N}\nabla^2_{\boldsymbol{r}_i} + V(\boldsymbol{R}, \boldsymbol{r}_1, \ldots, \boldsymbol{r}_N) - \frac{\hbar^2}{2\mu}\nabla^2_{\boldsymbol{R}} + \hat{H}', \tag{12}$$

where m_e is the electron mass and $V(\boldsymbol{R}, \boldsymbol{r}_1, \ldots, \boldsymbol{r}_N)$ is the Coulomb potential energy for the nuclei and electrons, which includes the electron-nucleus, electron-electron, and nucleus-nucleus interactions. The sum of the first two terms is the electronic Hamiltonian and the last term $\hat{H}'$ is neglected in the Born-Oppenheimer approximation. Only the first term in $\hat{H}'$ [Eq. (9)],

$$\hat{H}_{g\text{-}u} = -\frac{\hbar^2}{2\mu_\alpha}\nabla_{\boldsymbol{R}} \cdot \sum_{i=1}^{N} \nabla_{\boldsymbol{r}_i}, \tag{13}$$

does not commute with the space-inversion operator for electrons in the nonrelativistic total Hamiltonian $\hat{H}$ [Eq. (12)]

[31]. The term $\hat{H}_{g\text{-}u}$ hence brings about the *g-u* interaction, which is well known to be forbidden under the Born-Oppenheimer approximation that the electron mass is negligible against nuclear masses (see Table 3.2 on p. 97 in Ref. [32]) and the $\hat{H}_{g\text{-}u}$ term is the origin of the breaking of the space-inversion symmetry for electrons. We note that the term $\hat{H}_{g\text{-}u}$ vanishes for H_2 and D_2 because of the fact that $M_a = M_b$, but does not vanish for HD. The *g-u* interactions consequently occur in HD through the $\hat{H}_{g\text{-}u}$ term in contrast to H_2 and D_2, and it is reasonable to assign the origin of the new dissociation channels responsible for the enhancement in $f_{2p2p}(Q_2\,{}^1\Pi_u(1))$ for HD to the *g-u* interactions.

We first consider the *g-u* interactions at an infinite internuclear distance because they were discussed for HD [31] and ^{6}Li^{7}Li [34,35] by means of the two-state problem, where one atom is in the ground electronic state and the other atom is in an excited state and the resultant potential energy curves hence split at the infinite internuclear distance depending on which one of the two atoms is in the excited state. In the present experiment, however, both the H and D atoms are in the $n = 2$ level and the resultant potential energy curves do not split at the infinite internuclear distance. According to the two-state problem, no energy splitting results in the vanishing of the coupling term; see, e.g., Eqs. (21) and (22) in Ref. [31]. The superposition between a gerade state and an ungerade state is not consequently brought about at an infinite internuclear distance for doubly excited states of HD correlating with $(n = 2) + (n = 2)$ pair states. We thus consider the *g-u* nonadiabatic transitions that are responsible for the enhancement in $f_{2p2p}(Q_2\,{}^1\Pi_u(1))$ for HD and take place around the crossing point of the gerade and ungerade potential energy curves of HD.

We take account of the homogeneous ($\Delta\Lambda = 0$) and heterogeneous ($\Delta\Lambda = \pm 1$) *g-u* nonadiabatic transitions because the *g-u* interaction due to the $\hat{H}_{g\text{-}u}$ term was reported between the nearly coincident rotational levels of the $EF\ {}^1\Sigma_g^+$ state and the $B\ {}^1\Sigma_u^+$ state and between those of the $EF\ {}^1\Sigma_g^+$ state and the $C\ {}^1\Pi_u$ state [48,49]. They are all singly excited states of HD molecules, and the magnitudes of the coupling matrix elements are on the order of cm^{-1} [49].

The g-u nonadiabatic transitions responsible for the enhancement in the oscillator strength for 2p + 2p pair formation in HD

The potential energy curves of the doubly excited Q_2 states of H_2 converging to the $H(n = 2) + H(n = 2)$ limit were studied in the range of internuclear distance longer than $3a_0$ up to the asymptotic van der Waals regime together with their dissociation limits [26]. The repulsive potential energy curves and resonance widths of the doubly excited Q_2 states were extensively calculated in the range of internuclear distance shorter than $6a_0$ [23]. Based upon the comprehensive discussion of the crossings and pseudocrossings of the potential energy curves of the doubly excited Q_2 states converging to the $H(n = 2) + H(n = 2)$ limit, we obtain a schematic diagram showing the possible doubly excited states and nonadiabatic transitions that may influence the values of $f_{2p2p}(Q_2\,{}^1\Pi_u(1))$ in the photoexcitation of H_2, HD, and D_2 to the $Q_2\ {}^1\Pi_u(1)$ state (see Fig. 3). The horizontal arrows in Fig. 3 represent both the adiabatic correlation between the doubly excited states and atom pair states [26] and the corresponding dissociation channels. The vertical arrows in Fig. 3 denote the nonadiabatic transitions occurring at the indicated internuclear distances R, with the red ones denoting the *g-u* nonadiabatic transitions due to the $\hat{H}_{g\text{-}u}$ term and the blue ones denoting the nonadiabatic transitions due to the radial coupling. The nonadiabatic transitions due to the rotational coupling are unlikely in the present study since the potential energy curves of the doubly excited states of hydrogen molecules are repulsive [21–28] and hence the axial recoil approximation [50] holds well. The blue channels starting from the $Q_2\ {}^1\Pi_u(1)$ state (the blue horizontal and blue vertical arrows) have been substantiated for H_2 and D_2 [20], but the adiabatic correlations of the $Q_2\ {}^1\Pi_u(1)$ and $Q_2\ {}^1\Pi_u(2)$ states have been reversed to those in Refs. [14,20] following Ref. [26]. In Fig. 3 the resonance width Γ at an internuclear distance of $6a_0$ is shown for each doubly excited state [23].

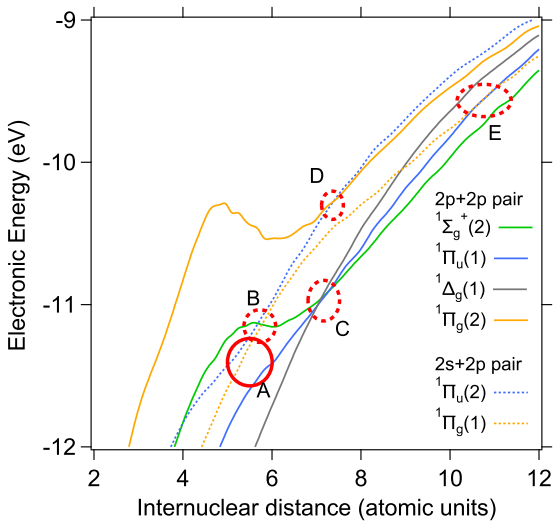

FIG. 4. Plot of electronic energies of the doubly excited states of H_2 in Fig. 3 against the internuclear distance [23,26]; the energies do not include the repulsive Coulomb potential energy between the two nuclei. The circles A–E show points of crossings or pseudocrossings between two curves (see the text for details). The nonadiabatic transitions A–E in Fig. 3 take place at the points labeled with the same letters. The origin of the energy is taken at an energy of $H^+ + H^+ + e^- + e^-$ and the electronic energies have no isotope effect.

The electronic energies of the doubly excited states in Fig. 3 are displayed against the internuclear distance in Fig. 4 (those in Refs. [23,26] for each state are smoothly connected, so a single curve is obtained for each state). We note that the electronic energies, which do not include the repulsive Coulomb interaction between the two nuclei, are plotted against the internuclear distance instead of the potential energy curves because the latter, which are the sum of the electronic energies and the repulsive Coulomb term, are repulsive and the energy range of the vertical axis becomes so wide that the details of the crossings and pseudocrossings between the curves become unclear. The dotted circles labeled B–E show crossing points between two curves and the

nonadiabatic transitions labeled B–E in Fig. 3 take place at the crossing points labeled the same letters. The closed circle labeled A shows the point of the pseudocrossing between the $Q_2\ ^1\Pi_u(1)$ and $Q_2\ ^1\Pi_u(2)$ curves and the nonadiabatic transition labeled A in Fig. 3 takes place there. This nonadiabatic transition from the $Q_2\ ^1\Pi_u(1)$ state to the $Q_2\ ^1\Pi_u(2)$ state plays a significant role in the decay dynamics of H_2 and D_2 molecules photoexcited to the $Q_2\ ^1\Pi_u(1)$ state [20] (as mentioned at the beginning of Sec. III) and this is also the case for HD.

We specify the *g-u* nonadiabatic transitions responsible for the enhancement in $f_{2p2p}(Q_2\ ^1\Pi_u(1))$ for HD seen in Fig. 2 from among possible ones in Figs. 3 and 4. It is noted that only transitions B and D are the *g-u* nonadiabatic transitions that convert the $2s+2p$ pairs to the $2p+2p$ pairs when HD molecules are photoexcited to the $Q_2\ ^1\Pi_u(1)$ state in the Franck-Condon region. We may hence show that the *g-u* nonadiabatic transition B or D, or both, following the nonadiabatic transition A from the $Q_2\ ^1\Pi_u(1)$ state to the $Q_2\ ^1\Pi_u(2)$ state, makes a major contribution to the enhancement in $f_{2p2p}(Q_2\ ^1\Pi_u(1))$ for HD from the value expected from $f_{2p2p}(Q_2\ ^1\Pi_u(1))$ for H_2 and D_2 (the plus on the dotted line in Fig. 2); this expectation is based on the assumption that the decay mechanisms of hydrogen molecules photoexcited to the $Q_2\ ^1\Pi_u(1)$ state are the same for H_2, HD, and D_2 (the blue arrows in Fig. 3). It was found in our recent experiment [20] that the oscillator strengths for $2s+2p$ pair formation from the $Q_2\ ^1\Pi_u(1)$ state of H_2 and D_2 are almost 6 times those for $2p+2p$ pair formation from the same state of H_2 and D_2, respectively. The populations of H_2 and D_2 in the $Q_2\ ^1\Pi_u(2)$ state (the blue horizontal dashed arrow in Fig. 3) are hence about 6 times the populations of H_2 and D_2 in the $Q_2\ ^1\Pi_u(1)$ state (the blue horizontal solid arrow in Fig. 3) at the infinite internuclear distance, respectively, which fact supports the present scenario just mentioned. It follows, according to Fig. 2 and the present scenario, that approximately 10–20 % of $f_{2p2p}(Q_2\ ^1\Pi_u(1))$ obtained in this study for HD arises from the *g-u* nonadiabatic transition B or D, or both, in Fig. 3 due to the $\hat{H}_{g\text{-}u}$ term.

IV. CONCLUSION

We have determined a set of cross sections for $2p+2p$ pair formation on an absolute scale against the incident photon energy in the range 30–40 eV in the photoexcitation of isotopomers H_2, HD, and D_2, incorporating the present cross sections with those of H_2 and D_2 obtained in our previous experiments [20], and the oscillator strengths of $2p+2p$ pair formation from the precursor doubly excited $Q_2\ ^1\Pi_u(1)$ state, $f_{2p2p}(Q_2\ ^1\Pi_u(1))$, have been determined from the cross sections. It is remarkable that $f_{2p2p}(Q_2\ ^1\Pi_u(1))$ for HD is larger than the value expected from $f_{2p2p}(Q_2\ ^1\Pi_u(1))$ for H_2 and D_2 (the plus on the dotted line in Fig. 2), which is based on the assumption that the decay mechanisms of hydrogen molecules photoexcited to the $Q_2\ ^1\Pi_u(1)$ state are the same for H_2, HD, and D_2 (the blue arrows in Fig. 3). We have discussed the origin of the enhancement in the oscillator strength for HD and shown that the enhancement in $f_{2p2p}(Q_2\ ^1\Pi_u(1))$ for HD is mainly attributed to the *g-u* nonadiabatic transitions from the $Q_2\ ^1\Pi_u(2)$ state correlating with the $2s+2p$ pair state to the gerade states correlating with the $2p+2p$ pair state, transitions which follow the nonadiabatic transition from the photoexcited $Q_2\ ^1\Pi_u(1)$ state to the $Q_2\ ^1\Pi_u(2)$ state. We note that those *g-u* nonadiabatic transitions do not occur in H_2 and D_2. It follows, according to Fig. 2 and the present scenario, that approximately 10–20 % of $f_{2p2p}(Q_2\ ^1\Pi_u(1))$ for HD originates from those *g-u* nonadiabatic transitions. The role of the *g-u* nonadiabatic transitions, i.e., the role of the breaking of the space-inversion symmetry for electrons, has been substantiated in the dynamics of HD molecules photoexcited to the doubly excited $Q_2\ ^1\Pi_u(1)$ state.

ACKNOWLEDGMENTS

The experiment was carried out under the approval of the Photon Factory Program Advisory Committee for Proposals No. 2014G108 and No. 2016G001. This work was supported by JSPS KAKENHI Grants No. JP15K05381 and No. JP17K05744. The authors thank Prof. J. L. Sanz-Vicario for sending us unpublished data.

[1] U. Fano, Phys. Rev. **124**, 1866 (1961).
[2] J. N. Bardsley, J. Phys. B **1**, 349 (1968).
[3] I. Sánchez and F. Martín, Phys. Rev. A **57**, 1006 (1998).
[4] A. Lafosse, M. Lebech, J. C. Brenot, P. M. Guyon, L. Spielberger, O. Jagutzki, J. C. Houver, and D. Dowek, J. Phys. B **36**, 4683 (2003).
[5] T. Odagiri, M. Murata, M. Kato, and N. Kouchi, J. Phys. B **37**, 3909 (2004).
[6] M. Glass-Maujean, S. Klumpp, L. Werner, A. Ehresmann, and H. Schmoranzer, J. Phys. B **37**, 2677 (2004).
[7] M. Glass-Maujean and H. Schmoranzer, J. Phys. B **38**, 1093 (2005).
[8] M. Glass-Maujean, R. Kneip, E. Flemming, and H. Schmoranzer, J. Phys. B **38**, 2871 (2005).
[9] E. M. García, J. A. Ruiz, S. Menmuir, E. Rachlew, P. Erman, A. Kivimäki, M. Glass-Maujean, R. Richter, and M. Coreno, J. Phys. B **39**, 205 (2006).
[10] F. Martin, J. Fernandez, T. Havermeier, L. Foucar, T. Weber, K. Kreidi, M. Schoffler, L. Schmidt, T. Jahnke, O. Jagutzki, A. Czasch, E. P. Benis, T. Osipov, A. L. Landers, A. Belkacem, M. H. Prior, H. Schmidt-Bocking, C. L. Cocke, and R. Dorner, Science **315**, 629 (2007).
[11] D. Dowek, J. F. Pérez-Torres, Y. J. Picard, P. Billaud, C. Elkharrat, J. C. Houver, J. L. Sanz-Vicario, and F. Martín, Phys. Rev. Lett. **104**, 233003 (2010).
[12] L. Ishikawa, T. Odagiri, K. Yachi, N. Ohno, T. Tsuchida, M. Kitajima, and N. Kouchi, J. Phys. B **44**, 065203 (2011).
[13] J. R. Machacek, V. M. Andrianarijaona, J. E. Furst, A. L. D. Kilcoyne, A. L. Landers, E. T. Litaker, K. W. McLaughlin, and T. J. Gay, J. Phys. B **44**, 045201 (2011).
[14] T. Odagiri, Y. Kumagai, M. Nakano, T. Tanabe, I. H. Suzuki, M. Kitajima, and N. Kouchi, Phys. Rev. A **84**, 053401 (2011).
[15] A. Medina, G. Rahmat, C. R. de Carvalho, G. Jalbert, F. Zappa, R. F. Nascimento, R. Cireasa, N. Vanhaecke, I. F. Schneider,

N. V. de Castro Faria, and J. Robert, J. Phys. B **44**, 215203 (2011).
[16] J. Robert, F. Zappa, C. R. de Carvalho, G. Jalbert, R. F. Nascimento, A. Trimeche, O. Dulieu, A. Medina, C. Carvalho, and N. V. de Castro Faria, Phys. Rev. Lett. **111**, 183203 (2013).
[17] Y. Nakanishi, K. Hosaka, R. Kougo, T. Odagiri, M. Nakano, Y. Kumagai, K. Shiino, M. Kitajima, and N. Kouchi, Phys. Rev. A **90**, 043405 (2014).
[18] A. Fischer, A. Sperl, P. Cörlin, M. Schönwald, S. Meuren, J. Ullrich, T. Pfeifer, R. Moshammer, and A. Senftleben, J. Phys. B **47**, 021001 (2014).
[19] K. Takahashi, Y. Sakata, Y. Hino, and Y. Sakai, Eur. Phys. D **68**, 83 (2014).
[20] K. Hosaka, K. Shiino, Y. Nakanishi, T. Odagiri, M. Kitajima, and N. Kouchi, Phys. Rev. A **93**, 063423 (2016).
[21] J. Tennyson, At. Data Nucl. Data Tables **64**, 253 (1996).
[22] I. Sánchez and F. Martín, J. Chem. Phys. **106**, 7720 (1997).
[23] I. Sánchez and F. Martıń, J. Chem. Phys. **110**, 6702 (1999).
[24] F. Martín, J. Phys. B **32**, L181 (1999).
[25] J. Fernández and F. Martín, J. Phys. B **34**, 4141 (2001).
[26] Y. V. Vanne, A. Saenz, A. Dalgarno, R. C. Forrey, P. Froelich, and S. Jonsell, Phys. Rev. A **73**, 062706 (2006).
[27] A. Igarashi and Y. Kuwayama, J. Phys. Soc. Jpn. **83**, 054302 (2014).
[28] A. Igarashi, J. Phys. B **48**, 105202 (2015).
[29] T. Odagiri, N. Uemura, K. Koyama, M. Ukai, N. Kouchi, and Y. Hatano, J. Phys. B **29**, 1829 (1996).
[30] N. Uemura, T. Odagiri, Y. Hirano, Y. Makino, N. Kouchi, and Y. Hatano, J. Phys. B **31**, 5183 (1998).
[31] A. D. Lange, E. Reinhold, and W. Ubachs, Int. Rev. Phys. Chem. **21**, 257 (2002).
[32] H. Lefebvre-Brion and R. W. Field, *The Spectra and Dynamics of Diatomic Molecules* (Academic, San Diego, 2004).
[33] K. Hosaka, Y. Torizuka, K. Minamizaki, P. Schmidt, A. Knie, A. Ehresmann, T. Odagiri, M. Kitajima, and N. Kouchi, Phys. Rev. A **98**, 052514 (2018).
[34] P. Cacciani and V. Kokoouline, Phys. Rev. Lett. **84**, 5296 (2000).
[35] N. Bouloufa, P. Cacciani, V. Kokoouline, F. Masnou-Seeuws, R. Vetter, and L. Li, Phys. Rev. A **63**, 042507 (2001).
[36] D. Rolles, M. Braune, S. Cvejanović, O. Geßner, R. Hentges, S. Korica, B. Langer, T. Lischke, G. Prümper, A. Reinköster, J. Viefhaus, B. Zimmermann, V. McKoy, and U. Becker, Nature (London) **437**, 711 (2005).
[37] K. Ito, Y. Morioka, M. Ukai, N. Kouchi, Y. Hatano, and T. Hayaishi, Rev. Sci. Instrum. **66**, 2119 (1995).
[38] K. Hosaka (private communication).
[39] K. P. Huber and G. Herzberg, *Molecular Spectra and Molecular Structure. IV. Constants of Diatomic Molecules* (Van Nostrand Reinhold, New York, 1979).
[40] J. L. Sanz-Vicario, H. Bachau, and F. Martín, Phys. Rev. A **73**, 033410 (2006).
[41] J. D. Bozek, J. E. Furst, T. J. Gay, H. Gould, A. L. D. Kilcoyne, J. R. Machacek, F. Martín, K. W. McLaughlin, and J. L. Sanz-Vicario, J. Phys. B **39**, 4871 (2006).
[42] J. L. Sanz-Vicario (private communication).
[43] H. Nakamura, J. Phys. Soc. Jpn. **26**, 1473 (1969).
[44] W. H. Miller, J. Chem. Phys. **52**, 3563 (1970).
[45] I. Borges and C. E. Bielschowsky, J. Phys. B **33**, 1713 (2000).
[46] P. Bunker, J. Mol. Spectrosc. **28**, 422 (1968).
[47] W. Kołos and L. Wolniewicz, Rev. Mod. Phys. **35**, 473 (1963).
[48] I. Dabrowski and G. Herzberg, Can. J. Phys. **54**, 525 (1976).
[49] P. C. Hinnen, S. E. Werners, S. Stolte, W. Hogervorst, and W. Ubachs, Phys. Rev. A **52**, 4425 (1995).
[50] R. N. Zare, Mol. Photochem. **4**, 1 (1972).